Nonlinear response of vertical paired structure in complex plasma

Zhiyue Ding, Ke Qiao, Jie Kong, Lorin Matthews and Truell W. Hyde
Center for Astrophysics, Space Physics and Engineering Research, Baylor University
Email: Zhiyue_Ding@baylor.edu,
Email: Ke_Qiao@baylor.edu,
Email: Truell_Hyde@baylor.edu.

The effect of the ion wake downstream of grains immersed in a flowing plasma is observed experimentally through the apparent non-reciprocal grain-grain interactions. Here we extend amplitude-frequency response analysis to examine the nonlinear components of the interaction of a dust particle pair aligned with the ion flow. The particle pair is modeled as two forced coupled oscillators, and a new coordinate system is introduced in which the breathing and sloshing modes are linearly decoupled. Multiple-scale analysis is used to derive analytical expressions for the response in the vertical direction for each mode in this coordinate system. By fitting the analytical expressions to experimentally measured response curves, the nonlinear part of the wake-modified particle-particle interaction is determined and identified as the source for the coupling between the sloshing and breathing modes. It is found that the restoring force acting on the downstream particle is more linear, thus stabilizing the oscillations of the downstream grain.

Keywords: complex plasma, non-reciprocal grain-grain interaction, ion wake, nonlinearity

1. INTRODUCTION

In a rf discharge plasma, dust particles levitated in the plasma sheath region are greatly influenced by the ion wake which is caused by the streaming ions scattered by the negatively charged dust[1]. For dust particles aligned with the ion flow, the ion wake field downstream of the dust particles lead to an asymmetric interaction potential between the grains [2–11]. Thus the ion wake plays an essential role in the dynamics of small grains in the plasma environment.

Numerical models of the ion wake including Particle-in-Cell (PIC) simulations [12–16], Monte Carlo simulation [17], or a combination of the two method [18], generally focus on the dynamics of the electrons and ions. These models have demonstrated that the wake potential behind dust grains takes a oscillating form which facilitates the alignment of dust particles below the upstream grains [13–15]. From the molecular dynamic point of view, the drag force from scattered ions stabilizes this alignment [17]. The charge of the downstream dust grains is also found to be decreased due to the wakefield [12, 16]. However, the dynamics of the dust particles affected by the ion wake are usually not included in the models. With static dust grain configurations in the models, it is not possible to test the grains response especially when there are multiple grains where the grain-grain interaction become dominant. Thus, the influence of the ion wake on the grain-grain interaction cannot be studied directly in simulations where the dust grain positions are fixed.

In experiment, it is possible to examine the ion wake in terms of the dynamics of the affected dust particles. A paired dust particle structure provides a suitable configuration to examine the ion wake as it is the simplest 1-D structure that can be formed which still involves all relevant coupling interaction [6, 19]. Experiments have confirmed the ion-wake-induced decharging effect [5, 20], and shown the instability triggered by the particle-particle interaction under the influence of ion wake [19, 21–25]. Using a linear approximation of the interaction force, Kong et al [26, 27] showed that the particle charge and effective Debye length could be measured by investigating the coupled oscillation of vertical dust pairs inside a glass box. Goree et al [28, 29] employed velocity distribution correlations to anlyze the oscillatory modes of dust particle pairs, which allowed them to examine the heating effect caused by the ion wake.

These previous experiments approximated the non-reciprocal particle-particle interaction by assuming a linear interaction potential. To better understand how the ion wake modifies the particle-particle interaction, it is necessary to extend the theory to the nonlinear regime. Nonlinear response analysis are so far limited to the dynamics of a single dust particle [30–32]. Ivlev et al [30] studied the nonlinear amplitude-frequency response for a single dust particle in order to test the anharmonic potential in the sheath of a low-pressure rf discharge. Zafiu et al [31] related the nonlinear response of a single particle to the position dependent charge variation as well as the asymmetric sheath potential. Wang et al [32] showed the effects that other sources can have on the nonlinear response of a single dust particle employing a technique numerically based on a model with self-consistently determined sheath field and dust charge. Shukla et al [33, 34] presented a mechanism for self excited large amplitude nonlinear oscillations at very low discharge pressure and studied the response of a dust grain attributing the parametric resonance to the plasma density oscillation by studying the response curves.

Here, we extend the nonlinear-amplitude frequency response analysis to a strongly coupled system with two degrees of freedom for the first time in dusty plasma, and apply amplitude-frequency response to measure the nonlinear contributions of the ion wake to the particle-

particle interaction force by studying the coupled motion of a dust particle pair structure aligned with the ion flow and confined within a glass box. Rather than considering the anharmonic sheath potential [30, 31], we instead take the particle-particle interaction as the main source of nonlinearity. We derive the analytical form of particles' motion governed by the nonlinear equations of motion using the multiple scale method, and compare with the experimentally measured response curves to determine the quadratic terms for both the upstream and downstream interaction forces.

2. THEORY

A confined, vertically paired dust particle structure under sinusoidal excitation of small amplitude and frequency Ω in a plasma discharge can be modeled as two forced coupled oscillators. At equilibrium, with the particle-particle interaction expanded to second order in the Taylor expansion (here the particle-particle interaction potential is not presumed to be of any specific form), the equations of motion in the vertical direction are

$$\begin{aligned} \ddot{x}_1 + \mu\dot{x}_1 + \omega_1^2 x_1 + k_1(x_1 - x_2) + k_1'(x_1 - x_2)^2 &= F_1 exp(i\Omega t) + cc, \\ \ddot{x}_2 + \mu\dot{x}_2 + \omega_2^2 x_2 + k_2(x_2 - x_1) + k_2'(x_2 - x_1)^2 &= F_2 exp(i\Omega t) + cc, \end{aligned} \tag{1}$$

where x_1 and x_2 are the displacements from equilibrium (1 and 2 being the indices for the upstream and downstream particles), μ is the neutral gas drag coefficient, ω_1 and ω_2 are the frequencies of the vertical confinements provided by the balance among the background electric field, gravity and the particle-particle interaction, k_1 and k_2 are the coefficients of the linear interaction between the particles, k_1' and k_2' are the coefficients of the second order terms in the Taylor expansion of the particle-particle interaction forces, F_1 and F_2 are amplitudes of the driving force. Here 'cc' stands for the complex conjugate (for conciseness, 'cc' will be dropped from the following derivations, while all solutions are understood to be accompanied by their complex conjugate components). In most cases, k_1 is not equal to k_2 for two particles aligned in a direction parallel to the ion flow, due to the non-reciprocal ion wake.

To solve these coupled nonlinear equations, we first eliminate the linear coupling terms in x_1 and x_2 by introducing a new coordinate system: $x_+ = x_1 - (\alpha_-)x_2$ and $x_- = x_1 - (\alpha_+)x_2$. Here α_+ (α_-) are the oscillation amplitude ratios for particles 1 and 2 corresponding to the breathing (sloshing) mode, which can be measured experimentally employing the Scanning Mode Spectra [35] technique (i.e., an extension of the traditional mode spectra technique where the motion of the two particles is projected onto all the possible eigenvectors). The original equations of motion can now be written in the decoupled form

$$\begin{aligned} \ddot{x}_+ + \mu\dot{x}_+ + \omega_+^2 x_+ + g_1(c_1 x_+ - c_2 x_-)^2 &= f_+ exp(i\Omega t) \\ \ddot{x}_- + \mu\dot{x}_- + \omega_-^2 x_- + g_2(c_1 x_+ - c_2 x_-)^2 &= f_- exp(i\Omega t). \end{aligned} \tag{2}$$

In Eq. (2) g_1, g_2, c_1, c_2 and f_+, f_- are related to the original parameters k_1', k_2', F_1 and F_2 through the relationships:

$$\begin{aligned} g_1 &= (k_1' - \alpha_- k_2')/(\alpha_+ - \alpha_-)^2, \\ g_2 &= (k_1' - \alpha_+ k_2')/(\alpha_+ - \alpha_-)^2, \end{aligned} \tag{3a}$$

$$\begin{aligned} c_1 &= \alpha_+ - 1, \\ c_2 &= \alpha_- - 1, \end{aligned} \tag{3b}$$

$$\begin{aligned} f_+ &= F_1 - \alpha_- F_2, \\ f_- &= F_1 - \alpha_+ F_2, \end{aligned} \tag{3c}$$

In the linear limit, Eq. (2) provides the equations of motion for the two oscillation modes, i.e., the breathing and sloshing mode, respectively. Their natural frequencies ω_+ and ω_- are directly measured by the SMS technique. In the rest of this paper, we will call x_+ (x_-) the breathing (sloshing) coordinate, α_+, α_- the decoupling parameters, and ω_+ and ω_- the frequencies of the breathing and sloshing modes.

The nonlinear equations in Eq. (2) can be solved using multiple scale perturbation theory by expanding a test solution across different time scales [36]. In this case, we assume an approximate solution keeping only terms to the order of $o(\epsilon^2)$ as:

$$\begin{aligned} x_+ &= \epsilon x_{+1}(t, t_1) + \epsilon^2 x_{+2}(t, t_1), \\ x_- &= \epsilon x_{-1}(t, t_1) + \epsilon^2 x_{-2}(t, t_1), \end{aligned} \tag{4}$$

where ϵ is a small dimensionless parameter that is used to indicate the order of approximation, x_{+1} and x_{-1} are approximate solutions to first order in ϵ, x_{+2} and x_{-2} are approximate solutions to second order in ϵ^2, and $t_1 = \epsilon t$ is the fast scale time. (See the Appendix A for the full derivation of Eq. (4) - Eq. (9).) Inserting these test solutions into Eq. (2) and equating terms at different orders of ϵ, the equations can now be solved independently for four different regions in terms of the driving frequency

Ω: primary breathing (sloshing) regions where Ω is close to the breathing (sloshing) mode frequency $\omega_+(\omega_-)$ and super-harmonic breathing (sloshing) regions where Ω is close to half the breathing (sloshing) frequency $\omega_+(\omega_-)$.

In the primary breathing region, $\Omega = \omega_+ + \delta\epsilon$, where δ is the deviation of the driving frequency Ω from the breathing mode frequency ω_+. The equations of motion to first order take the form:

$$\begin{aligned} &\frac{\partial^2 x_{+1}}{\partial t^2} + \omega_+^2 x_{+1} = 0, \\ &\frac{\partial^2 x_{-1}}{\partial t^2} + \omega_-^2 x_{-1} = f_- exp(i\Omega t), \end{aligned} \tag{5}$$

with the solution:

$$\begin{aligned} x_{+1} &= Aexp(i\Omega t), \\ x_{-1} &= Bexp(i\Omega t) + \frac{f_-}{-\Omega^2 + \omega_-^2} exp(i\Omega t), \end{aligned} \tag{6}$$

while the equations of motion in second order (ϵ^2) take the form:

$$\begin{aligned} \frac{\partial^2 x_{+2}}{\partial t^2} + \omega_+^2 x_{+2} &= -2\frac{\partial^2 x_{+1}}{\partial t \partial t_1} - \mu \frac{\partial x_{+1}}{\partial t} - g_1(c_1 x_{+1} - c_2 x_{-1})^2 + f_+ exp(i\Omega t), \\ \frac{\partial^2 x_{-2}}{\partial t^2} + \omega_-^2 x_{-2} &= -2\frac{\partial^2 x_{-1}}{\partial t \partial t_1} - \mu \frac{\partial x_{-1}}{\partial t} - g_2(c_1 x_{+1} - c_2 x_{-1})^2, \end{aligned} \tag{7}$$

It is well known that linear undamped theory predicts unbounded oscillations when Ω is equal to ω_+, irrespective of the excitation amplitude. However, in an actual experimental system these oscillations are generally finite, limited by damping and nonlinearities within the system. Thus, to obtain an uniformly valid approximate solution it is necessary to consider the excitation term (when at resonance) to the same order of ϵ used for the damping and all other nonlinearities [36]. In this case, at breathing resonance the excitation term in the breathing coordinate $f_+ exp(i\Omega t)$ appears in the equation of motion to second order in ϵ (Eq. (7)) where both damping and nonlinearity come into effect, while the excitation term in the sloshing coordinate $f_- exp(i\Omega t)$ appears in the equation of motion to first order in ϵ (Eq. (6)). Substituting the first order solution shown in Eq. (6) into the second order equations of motion given in Eq. (7) and eliminating the secular terms, A and B are found to be given by

$$\begin{aligned} A &= \frac{f_+}{i\omega_+(\mu + i2\delta\epsilon)} exp(i\delta t_1) + Cexp(-\frac{\mu t_1}{2}), \\ B &= C' exp(-\frac{\mu t_1}{2}), \end{aligned} \tag{8}$$

where C and C' are constants determined by initial conditions. In this entire derivation, the situation of internal resonance $\omega_+ \approx 2\omega_-$ is avoided, i.e., the possibility of the breathing mode being excited directly by the sloshing resonance is theoretically prohibited.

Substituting Eq. (8) into Eq. (6), the solutions for the primary breathing region yield:

$$\begin{aligned} x_{+1} =& \frac{-f_+}{\omega_+[\mu^2 + 4(\Omega - \omega_+)^2]^{\frac{1}{2}}} exp(i[\Omega t + arctg(\frac{\mu}{2(\Omega - \omega_+)})]) \\ &+ Cexp(-\frac{\mu t_1}{2} + i\omega_+ t), \end{aligned} \tag{9a}$$

$$x_{-1} = \frac{f_-}{-\Omega^2 + \omega_-^2} exp(i\Omega t) + C' exp(-\frac{\mu t_1}{2} + i\omega_- t). \tag{9b}$$

Following the same procedure, the solutions for the primary sloshing region to first order of approximation take the form:

$$x_{+1} = \frac{f_+}{-\Omega^2 + \omega_+^2} exp(i\Omega t) + Cexp(-\frac{\mu t_1}{2} + i\omega_+ t), \tag{10a}$$

$$\begin{aligned} x_{-1} =& \frac{-f_-}{\omega_-[\mu^2 + 4(\Omega - \omega_-)^2]^{\frac{1}{2}}} exp(i[\Omega t + arctg(\frac{\mu}{2(\Omega - \omega_-)})]) \\ &+ C' exp(-\frac{\mu t_1}{2} + i\omega_- t). \end{aligned} \tag{10b}$$

The relationship of the primary breathing response x_{+1} to the driving frequency is given by the first term in Eq. (9a), while the primary sloshing response x_{-1} is given by the first term in Eq. (10b). The second term in each of these equations is a transient response corresponding to the natural frequencies of each mode. As can be seen, to first order of approximation, the primary responses are independent of the nonlinear parameters g_1 and g_2. Therefore at a presumed low excitation amplitude (i.e., where only quadratic nonlinearity is considered) the primary response behavior is linear.

In the super-harmonic breathing (sloshing) regions, since there is no primary resonance (i.e., Ω is not close to either ω_+ or ω_-), all excitations need only be considered to first order of ϵ, i.e., all excitation terms should appear only to first order in the equations of motion. Following the same procedure as before, we find the solution for the secondary breathing region to be:

$$
\begin{aligned}
x_{+1} = & -\frac{g_1[c_1(\frac{f_+}{-\Omega^2+\omega_+^2}) - c_2(\frac{f_-}{-\Omega^2+\omega_-^2})]^2}{\omega_+[\mu^2+4(2\Omega-\omega_+)^2]^{\frac{1}{2}}} \\
& \times exp(i[2\Omega t + arctg(\frac{\mu}{2(2\Omega-\omega_+)})]) \\
& + \frac{f_+}{-\Omega^2+\omega_+^2} exp(i\Omega t) + C exp(-\frac{\mu t_1}{2} + i\omega_+ t),
\end{aligned} \tag{11a}
$$

$$
x_{-1} = \frac{f_-}{-\Omega^2+\omega_-^2} exp(i\Omega t) + C' exp(-\frac{\mu t_1}{2} + i\omega_- t), \tag{11b}
$$

while for the secondary sloshing region:

$$
x_{+1} = \frac{f_+}{-\Omega^2+\omega_+^2} exp(i\Omega t) + C exp(-\frac{\mu t_1}{2} + i\omega_+ t), \tag{12a}
$$

$$
\begin{aligned}
x_{-1} = & -\frac{g_2[c_1(\frac{f_+}{-\Omega^2+\omega_+^2}) - c_2(\frac{f_-}{-\Omega^2+\omega_-^2})]^2}{\omega_-[\mu^2+4(2\Omega-\omega_-)^2]^{\frac{1}{2}}} \\
& \times exp(i[2\Omega t + arctg(\frac{\mu}{2(2\Omega-\omega_-)})]) \\
& + \frac{f_-}{-\Omega^2+\omega_-^2} exp(i\Omega t) + C' exp(-\frac{\mu t_1}{2} + i\omega_- t).
\end{aligned} \tag{12b}
$$

The secondary responses corresponding to twice the excitation frequencies 2Ω can be clearly seen in Eq. (11a) and Eq. (12b) as the first terms in x_{+1} (Eq. (11a)) and x_{-1} (Eq. (12b)). In contrast to the primary responses, secondary responses are governed by the nonlinear parameters g_1 and g_2. Therefore, a secondary response with shifted phase can be considered as a direct consequence of the nonlinear particle-particle interaction.

3. EXPERIMENT

The experiment discussed here was conducted in a modified Gaseous Electronics Conference (GEC) RF reference cell. The lower electrode was powered at 13.56 MHz while the upper electrode was grounded. A 20 mm × 18 mm × 18 mm (height × length × width) glass box was placed on the lower electrode in order to provide the horizontal confinement required to form vertical chain structures. Melamine Formaldehyde (MF) particles with diameter of $8.89 \pm 0.09\ \mu m$ were dropped into the plasma through a shaker mounted above the upper electrode, and levitated inside the glass box. Initially, a long chain structure inside the box was formed at a plasma power of 1.96 W. By carefully reducing the plasma power, dust particles were dropped to the bottom electrode until only two were left in the box. Once a paired structure was formed, the plasma power was increased to its experimental value, 9.82 W, where the small inter-particle distance results in a strongly coupled pair structure.

A function generator coupled to the lower electrode through an 20 dB attenuator was employed to provide a sinusoidal driving force to the particle pair. During the experiment, the driving frequency of the lower electrode was increased from 1 Hz to 50 Hz in steps of 0.1 Hz under a constant driving amplitude of 1 V. The trajectories of the vertically aligned particles at each step were recorded from the side using a high speed CCD camera at 500 frames per second to collect a total of 5000 frames. Throughout the experiment, the gas pressure was held at 40 mTorr, ensuring detection of particle thermal motion, while the plasma power was maintained at 9.82 W.

A. Mode decoupling in the sloshing and breathing coordinate

Since the particle pair is driven vertically, all the analysis here is based on the particles' vertical motion. Typically the analysis is done using the coordinate of the center of mass and positions relative to the center of mass. The motion of the center of mass is commonly related to the sloshing mode of the particle oscillation, while the relative coordinate is related to the breathing mode. However Fast Fourier Transformation (FFT) of the time series of particles' thermal center of mass motion and relative motion, Fig. 1a and Fig. 1c show that there is considerable response at the sloshing frequency for the relative coordinate, and considerable response at the breathing frequency for the center of mass coordinate. The non-reciprocal property of the particle-particle interaction (i.e., $k_1 \neq k_2$) causes the center of mass mode basis set to no longer be orthogonal to the relative mode basis set. It is reasonable to observe both sloshing and breathing components in the center of mass and the relative coordinates, since they characterize the 'pure' sloshing mode (i.e., where the particles are oscillating in phase with the same amplitude of motion) and the 'pure' breathing mode (i.e., where the particles are oscillating 180 degrees out of phase with the same amplitude of motion), respectively.

To separate the different modes in the linear regime for dust particles with nonreciprocal interaction, it is necessary to apply the sloshing and breathing coordinates introduced in Section II. Fig. 2 shows the Scanning Mode Spectra (SMS) obtained from the particle thermal motion [35]. The mode frequencies ω_+, ω_- and decou-

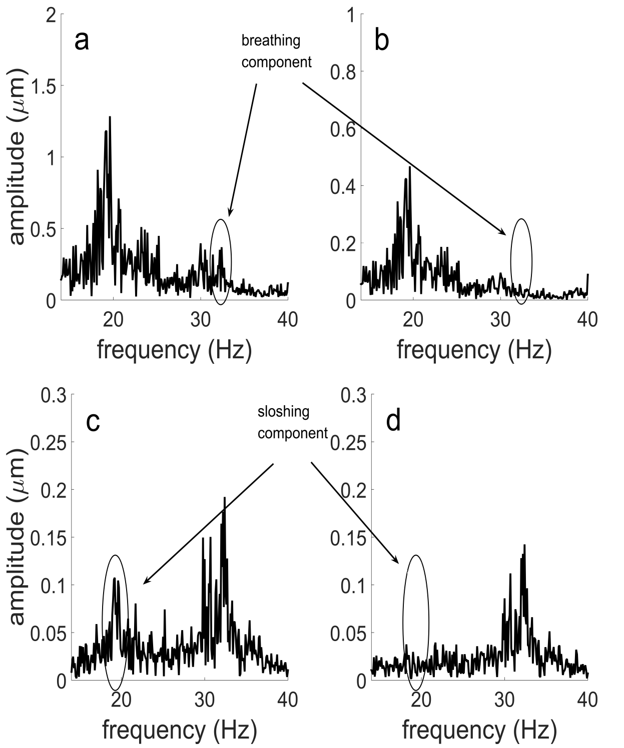

FIG. 1. Fast Fourier Transform (FFT) of the thermal motion of a particle pair for a) the conventional center of mass coordinate $(x_1 + x_2)$, b) the sloshing coordinate $(x_1 - \alpha_+ x_2)$, c) the relative coordinate $(x_1 - x_2)$ and d) the breathing coordinate $(x_1 - \alpha_- x_2)$.

pling parameters α_+ and α_- (i.e., the oscillation amplitude ratio) for the two modes were directly measured from the maxima in the SMS at the higher (ω_+) and lower (ω_-) frequencies. The oscillation amplitude ratios $\alpha_+(= -0.35)$ and $\alpha_-(= 0.81)$ can now be used to transform the recorded time series of trajectories $x_1(t)$ and $x_2(t)$ for the upstream and downstream particles into decoupled coordinates $x_+(t) = x_1(t) - (\alpha_-)x_2(t)$ and $x_-(t) = x_1(t) - (\alpha_+)x_2(t)$. The FFTs of the particles' thermal motion in the sloshing and breathing coordinates are shown in Fig. 1b and Fig. 1d, where the the undesired component (i.e., the breathing component in the sloshing coordinate and the sloshing component in the breathing coordinate) is elimated from each mode. Note that there are some frequency components appearing around 30 Hz which comes from the intrinsic system noise in our GEC reference cell (probably the cyclic cooling pump), which should be distinguished from the breathing component at 32 Hz. From the experimentally measured values of ω_+, ω_-, α_+ and α_-, the linear coefficients and vertical confinements in Eq.(1) are calculated to be $k_1 = 6733\ s^{-2}$ and $k_2 = 22368\ s^{-2}$, $\omega_1 = 19.2$ Hz and $\omega_2 = 16.2$ Hz.

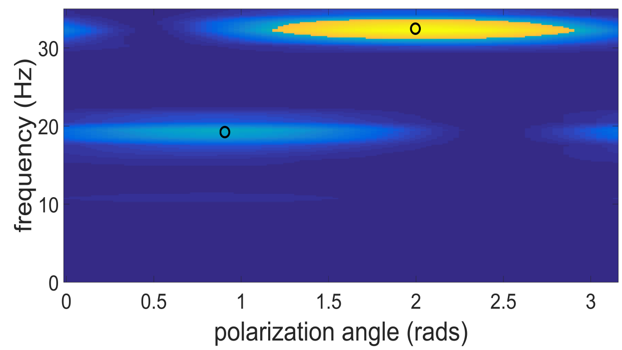

FIG. 2. Scanning Mode Spectra for the particles' thermal motion. The sloshing mode frequency ω_- is approximately 18.5 Hz with polarization $\phi_- = 1.05$ [35]. The breathing mode frequency ω_+ is approximately 32 Hz with polarization $\phi_+ = 1.91$. Decoupling parameters can be determined by taking the cotangent of the polarizations, $\alpha_- = cot(\phi_-)$ and $\alpha_+ = cot(\phi_+)$.

B. Experimental measurement of response curves

Primary and secondary responses can be determined experimentally by driving the particle pair at a frequency Ω and then calculating the FFT of the particles' motion in the decoupled coordinates $x_-(t)$ and $x_+(t)$. A representive example is shown in Fig. 3, where FFT's for both the sloshing coordinate (3a) and breathing coordinate (3b) are shown for a particle pair driven at 8.5 Hz. Strong peaks, the primary response, appear at 8.5 Hz (Ω) in both coordinates, accompanied by relatively weak peaks at the secondary response at 17 Hz (2Ω). Designating the amplitude of the peaks corresponding to the primary and secondary response at varying driving frequencies as $P(\Omega)$ and $S(\Omega)$, the primary and secondary response curves as a function of Ω can be obtained experimentally.

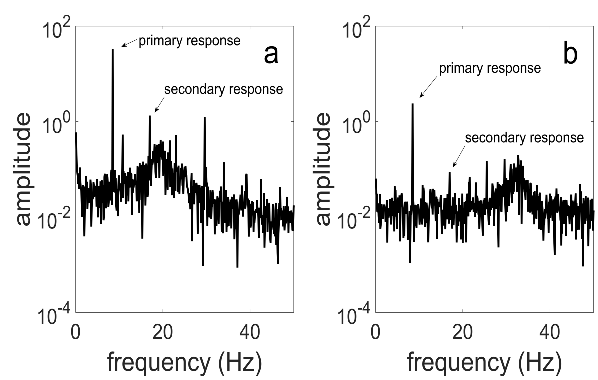

FIG. 3. Dust particle pair driven at 8.5 Hz. a) FFT of the sloshing coordinate. b) FFT for the breathing coordinate.

It is important to note that there appears to be a contradiction between the analytical solutions given in Eqs.

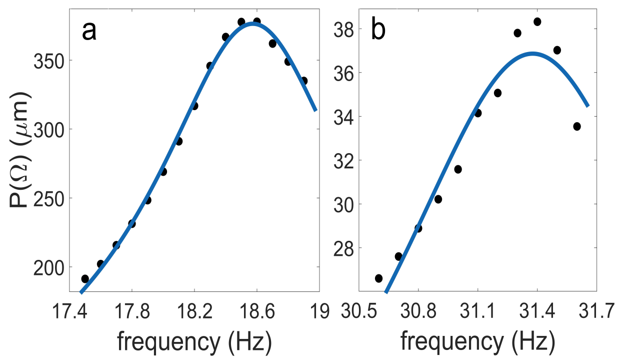

FIG. 4. Primary response curves for a) sloshing coordinate and b) breathing coordinate. The points are experimental data while the lines are fits to the analytical solution (i.e., first terms in Eq. (9a) and Eq. (10b)).

(9)-(12) and the experimental observations. For the analytical solutions, the responses at the natural frequencies ω_+ and ω_- are transient terms which decay as time increases. However, in experimental observations, these transient components remain throughout (Fig. 3). This contradiction is reconciled by noting that under actual experimental conditions, there are always thermal excitations (kicks) such that the response reaches a steady state.

4. RESULTS

A. Determination of the particle-particle interaction to the nonlinear regime

The obtained experimental primary response curves can be fitted by the theoretical primary responses (as given by Eqs. (9)-(12)). Fig. 4 shows fits to the primary responses in sloshing (Fig. 4(a)) and breathing (Fig. 4(b)) coordinates under these conditions. Since the parameters ω_+ and ω_- have already been determined from the SMS, there are only two parameters, μ and f_+ (f_-), left to be determined from each fit. As such, these fits yield a drag coefficient [37] of $\mu = 7.7\ s^{-1}$ within the primary sloshing region and $\mu = 9.0\ s^{-1}$ for the primary breathing region, in agreement with the value of $\mu = 8.5 \pm 0.9\ s^{-1}$ as measured employing a free fall technique [38, 39]. This allows values for $f_+$and f_- to be determined from the fit as $f_+ = 0.67 \times 10^5\ \mu m \cdot s^{-2}$ and $f_- = 3.34 \times 10^5\ \mu m \cdot s^{-2}$, respectively.

Before these fits can be employed to determine the secondary responses, the relative phase of the decoupled driving forces $f_1 exp(i\Omega t)$ and $f_2 exp(i\Omega t)$ must first be identified, i.e., whether f_1 and f_2 are of the same or opposite sign. This clarification can be made by taking advantage of the following experimental observation: at lower driving frequencies the magnitude of the oscillation of the upstream particle is larger than that of the downstream particle, while at higher frequencies the situation is reversed. Fig. 5 shows experimentally measured oscillation amplitudes for both the upstream and downstream particles. The blue line corresponds to the upstream particle $x_1(t)$ while the dashed red line corresponds to the downstream particle $x_2(t)$. A transition point can be observed at a driving frequency of approximately 34 Hz.

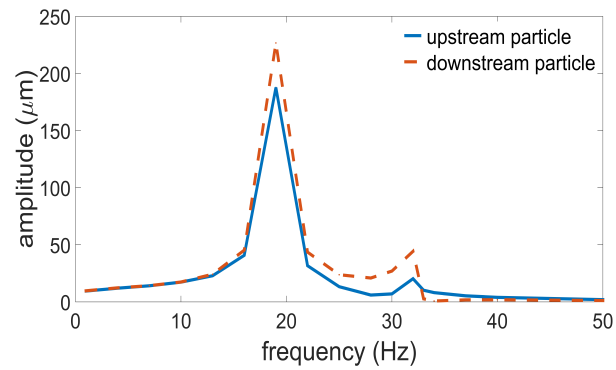

FIG. 5. Experimental measurement of the oscillation amplitudes (primary responses) for both the upstream (blue solid line) and downstream particle (red dashed line).

This phenomenon can be explained theoretically by solving the equations of motion for two linear forced coupled oscillators (see Eq. (1) without the nonlinear interaction terms $k_1'(x_1 - x_2)^2$ and $k_2'(x_1 - x_2)^2$). The nonlinear terms have little effect on the primary responses observed under small excitation amplitudes, as discussed in Section II. The ratio R between the response amplitudes of the upstream and downstream particle can thus be derived from the linear equations of motion as

$$R = \frac{\{[F_1(-\Omega^2 + k_2 + \omega_2^2) + k_1 F_2][F_2(-\Omega^2 + k_1 + \omega_1^2) + k_2 F_1] + \mu^2\Omega^2 F_1 F_2\}}{[F_2(-\Omega^2 + k_1 + \omega_1^2) + k_2 F_1]^2 + (\mu\Omega F_2)^2} + i\mu\Omega \frac{\{F_1[F_2(-\Omega^2 + k_1 + \omega_1^2) + k_2 F_1] - F_2[F_1(-\Omega^2 + k_2 + \omega_2^2) + k_1 F_2]\}}{[F_2(-\Omega^2 + k_1 + \omega_1^2) + k_2 F_1]^2 + (\mu\Omega F_2)^2}. \tag{13}$$

For simplification we drop the damping terms in Eq. (13). This can be justified since the damping is of the same order of magnitude as the nonlinear force contribution. Therefore, neglecting the damping does not qualitatively affect the result. By doing so, the amplitude ratio now reduces to

$$R = \frac{\eta(-\Omega^2 + k_2 + \omega_2^2) + k_1}{(-\Omega^2 + k_1 + \omega_1^2) + \eta k_2}, \tag{14}$$

where $\eta = \frac{F_1}{F_2}$ is defined as the ratio between the amplitudes of the excitation forces. Once f_+ and f_- are determined from fitting the measured primary response (as shown in Fig. 4), F_1 and F_2 are found using Eq. (3c). For the response fits shown in Fig. 4, this allows η to be calculated to be 0.62 when f_+ and f_- are of the opposite sign (i.e., out of phase case) and 1.1 when f_+ and f_- are of the same sign (i.e., in phase case). Based on the parameters k_1, k_2, ω_1 and ω_2 determined by employing the SMS method, the frequency ranges where the oscillation amplitude for the upstream particle is larger than that for the downstream particle (i.e., $R > 1$) can now be calculated from Eq. (14). This frequency range takes different form depending on the value of η, and it is also conditional on whether $\omega_1^2 - \omega_2^2$ is greater or less than $\frac{1-\eta}{\eta}(k_1 + \eta k_2)$:

$$\Omega^2 \in (-\infty, \frac{\omega_1^2 - \eta\omega_2^2}{1-\eta}) \cup (k_1 + \eta k_2 + \omega_1^2, +\infty), \eta > 1 \tag{15a}$$

$$\Omega^2 \in (\frac{\omega_1^2 - \eta\omega_2^2}{1-\eta}, k_1 + \eta k_2 + \omega_1^2), 0 < \eta < 1 \tag{15b}$$

For the situation $\eta > 1$ (i.e., in-phase driving), $\omega_1^2 - \omega_2^2$ is found to be greater than $\frac{1-\eta}{\eta}(k_1 + \eta k_2)$ based on the experimental parameters derived for k_1, k_2, ω_1, and ω_2. The corresponding frequency range that the oscillation of the upstream particle is larger than that for the downstream particle ($R > 1$) is predicted by Eq. 15a to be $\Omega > 34$ Hz, while for the situation $0 < \eta < 1$ (i.e., out of phase driving), $\omega_1^2 - \omega_2^2$ is less than $\frac{1-\eta}{\eta}(k_1 + \eta k_2)$ leading to a frequency range described in Eq. 15b as 24 Hz $\leq \Omega \leq$ 30 Hz. Thus the predicted result for in-phase driving agrees with the observed experimental response shown in Fig. 5, and we can conclude that f_+ and f_- are of the same sign. As a side result, it is determined that the driving force on the upstream particle is greater than that acting on the downstream particle, $F_1 > F_2$, in agreement with results reported by Carstensen et al [10].

With f_+ and f_- now determined, the experimentally determined secondary response curve can be compared to the theoretically derived secondary response (Eq. (11) and Eq. (12)). The fits with experiment are shown for the sloshing coordinate with $\Omega \approx \frac{1}{2}\omega_-$ in Fig. 6(a), while the fit for the breathing coordinate with $\Omega \approx \frac{1}{2}\omega_+$ is shown in Fig. 6(b). Since the secondary responses are smaller than our camera resolution of 9.0 μm per pixel, the errorbar caused by this uncertainty in measurement is shown in Fig. 6. Here the free parameters in each fit are g_1 and g_2, which are determined to be $g_1 = 283.2$ $\mu m^{-1}s^{-2}$ and $g_2 = 31.1$ $\mu m^{-1}s^{-2}$ respectively. The nonlinear coefficients k_1' and k_2' are then in turn calculated to be -253.4 $\mu m^{-1}s^{-2}$ and -364.6 $\mu m^{-1}s^{-2}$ from Eq. (3a).

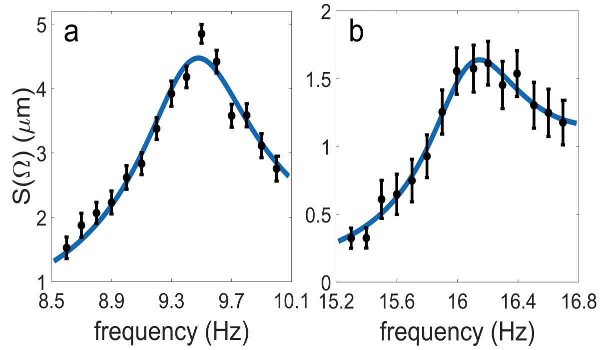

FIG. 6. Fits for the measured secondary responses a) in the sloshing coordinate at $\frac{1}{2}\omega_-$ and b) breathing coordinate at $\frac{1}{2}\omega_+$ to the analytical response curves. The points show experimental data while the solid lines are fits using the theoretical solutions (i.e., first terms in Eq. (11a) and Eq. (12b)). The errorbars are calculated from the measurement uncertainty due to the resolution of the camera which is 9 micrometers per pixel.

B. Numerical results

Additional simulations were conducted to validate the calculated values for k_1' and k_2' above. In this case, particle motions were simulated using a Velocity Verlet Algorithm based on the parameters ω_1, ω_2, k_1 and k_2 measured from the SMS technique and μ, F_1, F_2, k_1' and k_2' calulated from the response fits. The particle motion was simulated for for purely linear interactions ($k_1' = k_2' = 0$) as well as non-linear interactions. The resulting time series for the particle positions was then processed using the same approach as for the experimental data to obtain simulated response functions. The primary responses for the $x_1(t)$ and $x_2(t)$ coordinates are shown in Fig. 7. As can be seen, the simulation agrees well with experiment (Fig. 5) and successfully reproduces the transition phenomenon at around 34 Hz. The primary responses with nonlinear interactions exhibit only slight deviations from those with only linear interactions. This supports the previous argument that for small excitation amplitudes, the primary response is only minimally affected by the nonlinear interaction.

Secondary responses obtained from simulations with nonlinear interaction are indicated by the dashed line in Fig. 8, for $\Omega \approx \omega_-$ (Fig. 8(a)) and $\Omega \approx \omega_+$ (Fig. 8(b)) for both the breathing ($x_+(t)$, red curves) and sloshing (x_-(t), blue curves) coordinates. The consistency of the simulation with experimental measurement (solid curves)

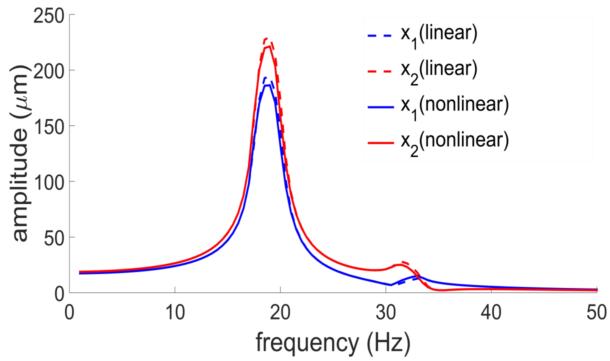

FIG. 7. Simulated response of upstream (blue) and downstream (red) particles. Solid lines show the results including the non-linear interaction terms, while the dashed lines show the response using only linear interaction terms.

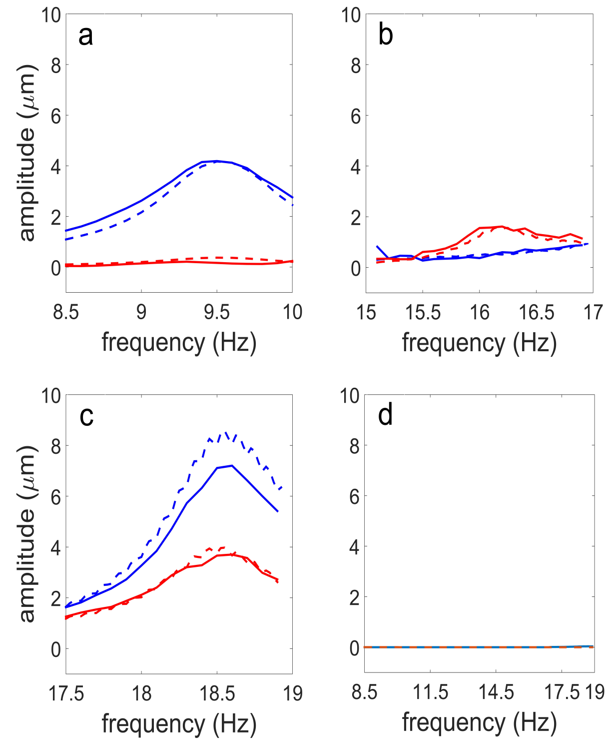

FIG. 8. Simulated secondary responses for a) the secondary sloshing region near $\frac{1}{2}\omega_-$ (around 9.5 Hz), b) the secondary breathing region near $\frac{1}{2}\omega_+$ (around 16 Hz) and c) the primary sloshing region near ω_- (around 18.5 Hz). Simulations including nonlinear interactions are plotted as dashed lines while experimental measurements are plotted as solid lines. Simulations which do not include nonlinear interactions ($k_1' = 0, k_2' = 0$) are plotted in Fig. 8(d). Lines plotted in blue represent sloshing coordinates and those plotted in red represent breathing coordinates.

confirms our calculation of the nonlinear coefficients k_1' and k_2'. Fig. 8(d) shows the simulation without considering nonlinear interaction, i.e., $k_1' = 0$ and $k_2' = 0$. As can be seen, when nonlinear interactions are not considered, there is no secondary response excited, indicating that secondary responses are purely caused by the nonlinear interactions. It is also interesting to note that both experiment and simulation show a secondary response in the breathing coordinate when the excitation frequency is around 18.5 Hz (the sloshing frequency ω_-) as shown in Fig. 8(c). Therefore, the breathing coordinate responds to the sloshing excitation. This is most likely a consequence of mode coupling in the nonlinear regime.

5. DISCUSSION

In this research, the restoring force due to the sheath potential is considered to be linear, leaving the source of nonlinearity to be attributed to the particle-particle interaction ($k_1'(x_1 - x_2)^2$ and $k_2'(x_2 - x_1)^2$) only. This assumption can be justified based on the findings of Tomme et al [40, 41], which showed that particle motion can be extremely well modeled by a damped harmonic oscillator for amplitudes approaching 20% of the sheath width. In this research, small particle vibration amplitudes are ensured through application of a low driving amplitude (1 V) through an attenuator. This provides a maximum vibration amplitude (appearing at the sloshing resonance) of less than 250 μm, which is estimated to be approximately 2% of the total sheath width. (The sheath edge is estimated to be at the plasma glow maxima.) As such, it is safe to assume a parabolic sheath potential (i.e., a linear electric field) and to ignore the effect of charge fluctuations.

Additionally, the maximum vibration amplitude in the breathing coordinate is less than 40 μm, which is small compared to the equilibrium interparticle spacing which is approximately 140 μm. Therefore, in theory, nonlinear effects in the particle-particle interaction beyond the quadratic term can be ignored. With this approximation both the theory (Eq. (9) and Eq. (10)) and simulation (Fig. 7) show that the primary response in both sloshing and breathing coordinates very weakly depends on the nonlinear coefficients k_1' and k_2'. Experimental results are in agreement with this conclusion, validiating the choice of neglecting higher order nonlinear terms.

Further increasing the excitation amplitude produces the spring hardening in the breathing coordinate, i.e., the resonance frequency shifts towards higher frequencies, which occurs as a consequence of a cubic nonlinearity. In fact, even under small excitations (e.g., the excitation in the presented experiment), the breathing mode is still slightly affected by the cubic nonlinearities, which is the reason that the primary breathing fit (Fig. 4a) is not as good as the primary sloshing fit (Fig. 4b). Interestingly, the spring hardening effect only appears in the breathing coordinate, while in the sloshing coordinate there is no obvious frequency shift. Since the breathing coordinate characterizes the particles' relative motion, this also confirms that the nonlinearity of the system arises from the particle-particle interaction rather than from the sheath, as discussed above. The situation of large excitation (significant spring hardening in the breathing coordinate created by the cubic nonlinearity) will be examined in future experiments.

Although the excitation (vibration amplitude) observed in the current research is small, secondary responses in both the sloshing and breathing coordinates are clearly seen. Since both theory and simulation show that these vanish for purly linear interactions, they serve as a signature of nonlinear particle-particle interactions.

It may be helpful here to compare our results to the case of a reciprocal particle-particle interaction and identical background confinement for both particles. Considering a reciprocal interaction ($k_1 = k_2 = k$, $k'_1 = -k'_2 = k'$) and identical confinement ($\omega_1 = \omega_2$) in Eq. (1), the modes are now orthogonal and $\alpha_+ = -1$ while $\alpha_- = 1$. For the ideal situation where both particles are driven identically, i.e., $F_1 = F_2 = F$, the external driving term disappears in the breathing coordinate while the driving magnitude equals $2F$ in the sloshing coordinate (Eq. (3c)). In this case, the breathing mode cannot be excited. However, in an actual experimental situation, any difference in the driving force or nonreciprocity in the particle-particle interaction can cause the breathing mode to become excited, in contrast to the result reported by Prior et al [42]. As seen in Eq. (3c), even when α_+/α_- deviates from -1 /1 (as is the case in the actual experiment), the effective driving force f_- is still much larger than f_+, explaining the much stronger primary response in the sloshing coordinate than in the breathing coordinate (see Fig. 4).

For $F_1 \neq F_2$, excitations of the two modes for a system with reciprocal interaction and an identical symmetric background confinement obey

$$\begin{aligned} \ddot{x}_+ + \mu\dot{x}_+ + \omega_+^2 x_+ + 2k' x_+^2 &= (F_1 - F_2) exp(i\Omega t), \\ \ddot{x}_- + \mu\dot{x}_- + \omega_-^2 x_- &= (F_1 + F_2) exp(i\Omega t). \end{aligned} \tag{16}$$

In this case, nonlinear terms only appear for the breathing coordinate, while the equation of motion for the sloshing coordinate remains linear. Comparing Eq. (16) to Eq. (2), we can conclude that it is the non-reciprocal interaction and the non-identical background confinement that couples the sloshing and breathing modes in a nonlinear manner. The secondary excitation observed in the sloshing coordinate is thus purely a consequence of this nonlinear coupling.

Finally, we define the nonlinearity length $L_1 = \frac{k_1}{k'_1}$ and $L_2 = \frac{k_2}{k'_2}$ as the ratio of the linear coefficients k_1, k_2 to the second order nonlinear coefficients k'_1, k'_2. This nonlinearity length L can be used as a measurement of nonlinearity scale for the particle-particle interaction. In this case, for the upstream force $L_1 = \frac{k_1}{k'_1} = -28$ μm and for the downstream force $L_2 = \frac{k_2}{k'_2} = -65$ μm. For comparison, we calculate L for a Yukawa potential as a function of the Debye length λ_D:

$$L_{Yukawa} = -\frac{2d\lambda_D^3 + 2d^2\lambda_D^2 + d^3\lambda_D}{6\lambda_D^3 + 6d\lambda_D^2 + 3d^2\lambda_D + d^3}, \tag{17}$$

where d is the inter-particle spacing at equilibrium (approximately 140 μm for this experiment). This L_{Yukawa} approaches an asymptotic value of $L = -\frac{d}{3}$ for large Debye length, which coresponds to the Coulomb interaction potential (i.e., $L_{Coulomb} = -\frac{d}{3}$). Fig. 9 shows nonlinearity length L_{Yukawa} for a particle separation $d = 140\mu m$ as a function of λ_D. It can be seen that the value for

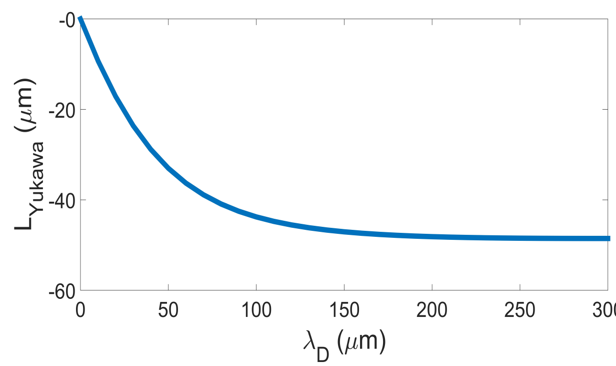

FIG. 9. The dependence of L_{Yukawa} on the Debye length λ_D for a Yukawa force with interparticle spacing $d = 140$ μm. As the Debye length increases, L_{Yukawa} asymptotically approaches the value for a Coulomb interaction with $L_{Coulomb} = -47$ μm.

the upstream particle, $L_1 = -28$ μm falls in the range where the Debye length λ_D equals approximately 1/3 of the inter-particle spacing, while the value for downstream nonlinearity length $L_2 = -65$ μm exceeds the asymptotic value $L = -47$ μm (corresponding to the Coulomb interaction). Thus, due to the ion wake, the downstream force is no longer a simple Yukawa or Coulomb interaction, even though the upstream force can still be described as an effective Yukawa interaction, in agreement with results reported in [43–46]. Furthermore, since $|L_1| < |L_2|$, it appears that the downstream interaction is more linear than the upstream. This implies that when the paired particles are at their equillibrium positions, the more linear restoring field for the downstream particle (effectively from the particle-particle interaction), results in more stable oscillations for the downstream particle.

6. CONCLUSIONS

A method to analyze nonlinear particle-particle interactions for a paired particle structure aligned with the ion flow in a complex plasma by experimentally measuring the nonlinear amplitude-frequency response curves has been presented. The method relies on examining the particle motion in a new coordinate system, the 'breathing' and 'sloshing' coordinates. Rewriting the system of equations for two coupled, forced oscillators in terms of these coordinates allows the sloshing and breathing modes to be linearly decoupled, as shown in Eq. (2) and illustrated in Fig. 1. The coupling in the nonlinear term is determined to result from the non-reciprocal particle interaction caused by the ion wake.

Multiple-scale analysis is used to solve the system of nonlinear coupled equations, and the motion is investigated for the primary response region (frequency near the driving frequency Ω) and the secondary response (frequency near 2Ω). The primary response in the breathing and sloshing coordinates are found to be independent of the nonlinear parameters (Eq. (9a) and Eq. (10b)), which only appear in the equations for the secondary response (Eq. (11a) and Eq. (12b)).

Amplitude-frequency response curves are obtained experimentally by applying a sinusoidally varying voltage to the lower electrode to drive the particles in the vertical direction. Fitting the primary response curve, determined from the amplitude of the FFT of the motion in the breathing and sloshing coordinates at the driving frequency Ω, with the analytical expression for the primary response allows the magnitude of the driving force and the damping parameter to be determined (Fig. 4). In turn, fitting the experimentally measured secondary response curves (Fig. 6) allows the coefficients of the non-linear coupling to be found.

Simulations of the particle motion using these measured parameters confirmed that the nonlinear terms contribute very little to the primary response of the system (Fig. 7), whereas excluding the nonlinear terms from the interaction completely eliminates the secondary response (Fig. 8). Thus, the existence of the secondary response can be taken as a signature of the nonlinearity present in the system. Non-reciprocal interactions or differences in the background confinement, as would be expected for a particle pair with the interaction mediated by the ion wake, results in equations of motion which are similar to the coupled driven oscillators (c.f. Eq. (2) and Eq. (16)). In this case, the coupling in the nonlinear term is determined to result from the apparent non-reciprocal particle-particle interaction caused by the ion wake. Further analysis shows that the nonlinear length scale, defined as the ratio of the coefficients of the linear and non-linear terms, is greater for the downstream particle. Thus the restoring force acting on the downstream particle is more linear than that acting on the upstream particle, stabilizing the oscillations of the downstream particle.

7. ACKNOWLEDGMENTS

Support from NASA grant number 1571701 and NSF grant number 1740203 is gratefully acknowledged.

Appendix A: Full derivation of the solutions at the primary breathing region

Consider the driving frequency near ω_+, i.e., $\Omega = \omega_+ + \delta\epsilon$. Writting out the drag force and the driving force at resonance to the same order in the nonliner terms (i.e., $\mu = \epsilon\mu'$, $f_+ = \epsilon^2 f'_+$, $f_- = \epsilon f'_-$), the equations of motion take the following form

$$\ddot{x}_+ + \epsilon\mu'\dot{x}_+ + \omega_+^2 x_+ + g_1(c_1 x_+ - c_2 x_-)^2 = \epsilon^2 f'_+ exp(i\Omega t) + cc, \tag{A1}$$

$$\ddot{x}_- + \epsilon\mu'\dot{x}_- + \omega_-^2 x_- + g_2(c_1 x_+ - c_2 x_-)^2 = \epsilon f'_- exp(i\Omega t) + cc. \tag{A2}$$

By substituting in the test solution

$$x_+(t_0, t_1) = \epsilon x_{+1}(t_0, t_1) + \epsilon^2 x_{+2}(t_0, t_1), \tag{A3}$$

$$x_-(t_0, t_1) = \epsilon x_{-1}(t_0, t_1) + \epsilon^2 x_{-2}(t_0, t_1), \tag{A4}$$

where $t_0 = t$ and $t_1 = \epsilon t_0$, the equations of motion to second order in ϵ are given by

$$\begin{aligned}&(\frac{\partial^2}{\partial t_0^2} + 2\epsilon\frac{\partial^2}{\partial t_0 \partial t_1} + \epsilon^2\frac{\partial^2}{\partial t_1^2})(\epsilon x_{+1} + \epsilon^2 x_{+2}) + \epsilon\mu'(\frac{\partial}{\partial t_0} + \epsilon\frac{\partial}{\partial t_1})(\epsilon x_{+1} + \epsilon^2 x_{+2})\\ &+ \omega_+^2(\epsilon x_{+1} + \epsilon^2 x_{+2}) + g_1[c_1(\epsilon x_{+1} + \epsilon^2 x_{+2}) - c_2(\epsilon x_{-1} + \epsilon^2 x_{-2})]^2 = \epsilon^2 f'_+ exp(i\Omega t_0) + cc,\end{aligned} \tag{A5}$$

$$\begin{aligned}&(\frac{\partial^2}{\partial t_0^2} + 2\epsilon\frac{\partial^2}{\partial t_0 \partial t_1} + \epsilon^2\frac{\partial^2}{\partial t_1^2})(\epsilon x_{-1} + \epsilon^2 x_{-2}) + \epsilon\mu'(\frac{\partial}{\partial t_0} + \epsilon\frac{\partial}{\partial t_1})(\epsilon x_{+1} + \epsilon^2 x_{+2})\\ &+ \omega_-^2(\epsilon x_{-1} + \epsilon^2 x_{-2}) + g_1[c_1(\epsilon x_{+1} + \epsilon^2 x_{+2}) - c_2(\epsilon x_{-1} + \epsilon^2 x_{-2})]^2 = \epsilon f'_- exp(i\Omega t_0) + cc.\end{aligned} \tag{A6}$$

The equations of motion are separated at different orders of ϵ, by equating all the terms of order of ϵ and ϵ^2, To first order in ϵ, the equations of motion are

$$\frac{\partial^2}{\partial t_0^2}x_{+1} + \omega_+^2 x_{+1} = 0, \tag{A7}$$

$$\frac{\partial^2}{\partial t_0^2}x_{-1} + \omega_-^2 x_{-1} = f'_- exp(i\Omega t_0) + cc, \tag{A8}$$

with the solution to the first order

$$x_{+1} = Aexp(i\omega_+ t_0) + cc, \tag{A9}$$

$$x_{-1} = Bexp(i\omega_- t_0) + \frac{f'_-}{-\Omega^2 + \omega_-^2} exp(i\Omega t_0) + cc. \tag{A10}$$

Equating the terms which are second order in ϵ yields

$$\frac{\partial^2}{\partial t_0^2}x_{+2} + \omega_+^2 x_{+2} = -2\frac{\partial^2}{\partial t_0 \partial t_1}x_{+1} - \mu' \frac{\partial}{\partial t_0}x_{+1} - g_1(c_1 x_{+1} - c_2 x_{-1})^2 + (f'_+ exp(i\Omega t_0) + cc), \tag{A11}$$

$$\frac{\partial^2}{\partial t_0^2}x_{-2} + \omega_-^2 x_{-2} = -2\frac{\partial^2}{\partial t_0 \partial t_1}x_{-1} - \mu' \frac{\partial}{\partial t_0}x_{-1} - g_2(c_1 x_{+1} - c_2 x_{-1})^2. \tag{A12}$$

Substituting x_{+1} and x_{-1} given by A9 and A10 into A11 and A12

$$\begin{aligned}
&\frac{\partial^2}{\partial t_0^2}x_{+2} + \omega_+^2 x_{+2} = -2i\omega_+ \frac{\partial A}{\partial t_1} exp(i\omega_+ t_0) - \mu' i\omega_+ Aexp(i\omega_+ t_0) + f'_+ exp(i\Omega t_0) \\
&- g_1[c_1^2 A^2 exp(i2\omega_+ t_0) + c_2^2 B^2 exp(i2\omega_- t_0) - 2c_1 c_2 ABexp(i(\omega_+ + \omega_-)t_0) \\
&- 2c_1 c_2 AB^* exp(i(\omega_+ - \omega_-)t_0) - 2c_1 c_2 A(\frac{f'_-}{-\Omega^2 + \omega_-^2})exp(i(\omega_+ + \Omega)t_0 \\
&- 2c_1 c_2 (\frac{f'_-}{-\Omega^2 + \omega_-^2})exp(i(\omega_+ - \Omega)t_0) + 2c_2^2 B(\frac{f'_-}{-\Omega^2 + \omega_-^2})exp(i(\omega_- + \Omega)t_0) \\
&+ 2c_2^2 B(\frac{f'_-}{-\Omega^2 + \omega_-^2})exp(i(\omega_- - \Omega)t_0) + c_2^2(\frac{f'_-}{-\Omega^2 + \omega_-^2})^2 exp(i2\Omega t_0) \\
&+ c_1^2 AA^* + c_2^2 BB^* + c_2^2(\frac{f'_-}{-\Omega^2 + \omega_-^2})^2] + cc,
\end{aligned} \tag{A13}$$

$$\begin{aligned}
&\frac{\partial^2}{\partial t_0^2}x_{-2} + \omega_-^2 x_{-2} = -2i\omega_- \frac{\partial B}{\partial t_1} exp(i\omega_- t_0) - \mu' i\omega_- Bexp(i\omega_- t_0) \\
&- \mu i\Omega(\frac{f'_-}{-\Omega^2 + \omega_-^2})exp(i\Omega t_0) - g_1[c_1^2 A^2 exp(i2\omega_+ t_0) + c_2^2 B^2 exp(i2\omega_- t_0) \\
&- 2c_1 c_2 ABexp(i(\omega_+ + \omega_-)t_0) - 2c_1 c_2 AB^* exp(i(\omega_+ - \omega_-)t_0) \\
&- 2c_1 c_2 A(\frac{f'_-}{-\Omega^2 + \omega_-^2})exp(i(\omega_+ + \Omega)t_0 - 2c_1 c_2(\frac{f'_-}{-\Omega^2 + \omega_-^2})exp(i(\omega_+ - \Omega)t_0) \\
&+ 2c_2^2 B(\frac{f'_-}{-\Omega^2 + \omega_-^2})exp(i(\omega_- + \Omega)t_0) + 2c_2^2 B(\frac{f'_-}{-\Omega^2 + \omega_-^2})exp(i(\omega_- - \Omega)t_0) \\
&+ c_2^2(\frac{f'_-}{-\Omega^2 + \omega_-^2})^2 exp(i2\Omega t_0) + c_1^2 AA^* + c_2^2 BB^* + c_2^2(\frac{f'_-}{-\Omega^2 + \omega_-^2})^2] + cc.
\end{aligned} \tag{A14}$$

Since $exp(i\Omega t_0) = exp(iw_+ t_0 + \delta t_1)$, where $\Omega = \omega_+ + \delta\epsilon$, then A13 and A14 become:

$$
\begin{aligned}
&\frac{\partial^2}{\partial t_0^2}x_{+2} + \omega_+^2 x_{+2} = [-2i\omega_+\frac{\partial A}{\partial t_1} - \mu' i\omega_+ A + f'_+ exp(i\delta t_1)]exp(i\omega_+ t_0) \\
&- g_1[c_1^2A^2 + c_2^2(\frac{f'_-}{-\Omega^2+\omega_-^2})^2 exp(i2\delta t_1) - 2c_1c_2A(\frac{f'_-}{-\Omega^2+\omega_-^2})exp(i\delta t_1)]exp(i2\omega_+ t_0) \\
&- g_1[2c_2^2B(\frac{f'_-}{-\Omega^2+\omega_-^2})exp(i\delta t_1) - 2c_1c_2AB]exp(i(\omega_+ + \omega_-)t_0) \\
&- g_1[2c_2^2B^*(\frac{f'_-}{-\Omega^2+\omega_-^2})exp(i\delta t_1) - 2c_1c_2AB^*]exp(i(\omega_+ - \omega_-)t_0) \\
&- g_1[c_1^2AA^* + c_2^2BB^* + c_2^2(\frac{f'_-}{-\Omega^2+\omega_-^2})^2 - 2c_1c_2A(\frac{f'_-}{-\Omega^2+\omega_-^2})exp(-i\delta t_1)] \\
&- g_1c_2^2B^2 exp(i2\omega_- t_0) + cc.
\end{aligned} \tag{A15}
$$

$$
\begin{aligned}
&\frac{\partial^2}{\partial t_0^2}x_{-2} + \omega_-^2 x_{-2} = (-2i\omega_-\frac{\partial B}{\partial t_1} - \mu' i\omega_- B)exp(i\omega_- t_0) - \mu' i\Omega(\frac{f_-}{-\Omega^2+\omega_-^2})exp(i\delta t_1)exp(i\omega_+ t_0) \\
&- g_2[c_1^2A^2 + c_2^2(\frac{f'_-}{-\Omega^2+\omega_-^2})^2 exp(i2\delta t_1) - 2c_1c_2A(\frac{f'_-}{-\Omega^2+\omega_-^2})exp(i\delta t_1)]exp(i2\omega_+ t_0) \\
&- g_2[2c_2^2B(\frac{f'_-}{-\Omega^2+\omega_-^2})exp(i\delta t_1) - 2c_1c_2AB]exp(i(\omega_+ + \omega_-)t_0) \\
&- g_2[2c_2^2B^*(\frac{f'_-}{-\Omega^2+\omega_-^2})exp(i\delta t_1) - 2c_1c_2AB^*]exp(i(\omega_+ - \omega_-)t_0) \\
&- g_2[c_1^2AA^* + c_2^2BB^* + c_2^2(\frac{f'_-}{-\Omega^2+\omega_-^2})^2 - 2c_1c_2A(\frac{f'_-}{-\Omega^2+\omega_-^2})exp(-i\delta t_1)] \\
&- g_2c_2^2B^2 exp(i2\omega_- t_0) + cc.
\end{aligned} \tag{A16}
$$

To ensure that there are no secular terms in the equations of motion for x_{+2} (A15) and x_{-2} (A16), the resonant terms on the right hand side of A15 and A16 are forced to be 'zero', allowing the coefficients A and B to be determined from

$$- 2i\omega_+\frac{\partial A}{\partial t_1} - \mu' i\omega_+ A + f'_+ exp(i\delta t_1) = 0, \tag{A17}$$

$$- 2i\omega_-\frac{\partial B}{\partial t_1} - \mu' i\omega_- B = 0, \tag{A18}$$

with the solutions

$$A = \frac{f'_+}{i\omega_+(\mu' + i2\delta)}exp(i\delta t_1) + cexp(-\frac{\mu' t_1}{2}), \tag{A19}$$

$$B = c' exp(-\frac{\mu' t_1}{2}). \tag{A20}$$

Thus, the solutions to first order in ϵ are found to be

$$
\begin{aligned}
x_+ =& \frac{-f_+}{\omega_+[\mu^2 + 4(\Omega - \omega_+)^2]^{\frac{1}{2}}} exp(i[\Omega t + arctg(\frac{\mu}{2(\Omega - \omega_+)})]) \\
&+ Cexp(-\frac{\mu t_1}{2} + i\omega_+ t) + cc,
\end{aligned} \tag{A21}
$$

$$x_- = \frac{f_-}{-\Omega^2 + \omega_-^2} exp(i\Omega t) + C' exp(-\frac{\mu t_1}{2} + i\omega_- t) + cc, \tag{A22}$$

where C and C' are constants depending on the initial conditions and 'cc' stands for the complex conjugate. The solutions for the other frequency regions are derived in a similar manner.

[1] V. Fortov, A. Ivlev, S. Khrapak, A. Khrapak, and G. Morfill, Physics Reports **421**, 1 (2005).
[2] A. Melzer, V. A. Schweigert, I. V. Schweigert, A. Homann, S. Peters, and A. Piel, Phys. Rev. E **54**, R46 (1996).
[3] V. A. Schweigert, I. V. Schweigert, A. Melzer, A. Homann, and A. Piel, Phys. Rev. E **54**, 4155 (1996).
[4] V. A. Schweigert, I. V. Schweigert, A. Melzer, A. Homann, and A. Piel, Phys. Rev. Lett. **80**, 5345 (1998).
[5] A. Melzer, V. A. Schweigert, and A. Piel, Phys. Rev. Lett. **83**, 3194 (1999).
[6] A. Melzer, V. A. Schweigert, and A. Piel, Physica Scripta **61**, 494 (2000).
[7] G. A. Hebner, M. E. Riley, and B. M. Marder, Phys. Rev. E **68**, 016403 (2003).
[8] A. A. Samarian, S. V. Vladimirov, and B. W. James, Physics of Plasmas **12**, 022103 (2005).
[9] J. Carstensen, F. Greiner, and A. Piel, Phys. Rev. Lett. **109**, 135001 (2012).
[10] A. V. Zobnin, A. P. Nefedov, V. A. Sinel'shchikov, O. A. Sinkevich, A. D. Usachev, V. S. Filinov, and V. E. Fortov, Plasma Physics Reports **26**, 415 (2000).
[11] A. Melzer, Plasma Sources Science and Technology **10**, 303 (2001).
[12] W. J. Miloch, M. Kroll, and D. Block, Physics of Plasmas **17**, 103703 (2010).
[13] I. H. Hutchinson, Physics of Plasmas **18**, 032111 (2011).
[14] I. H. Hutchinson, Phys. Rev. Lett. **107**, 095001 (2011).
[15] I. H. Hutchinson, Phys. Rev. E **85**, 066409 (2012).
[16] W. J. Miloch and D. Block, Physics of Plasmas **19**, 123703 (2012).
[17] A. Piel, Physics of Plasmas **18**, 073704 (2011).
[18] V. R. Ikkurthi, K. Matyash, A. Melzer, and R. Schneider, Physics of Plasmas **17**, 103712 (2010).
[19] A. Melzer, Phys. Rev. E **90**, 053103 (2014).
[20] H. Jung, F. Greiner, O. H. Asnaz, J. Carstensen, and A. Piel, Physics of Plasmas **22**, 053702 (2015).
[21] V. Steinberg, R. Sütterlin, A. V. Ivlev, and G. Morfill, Phys. Rev. Lett. **86**, 4540 (2001).
[22] R. Kompaneets, S. V. Vladimirov, A. V. Ivlev, V. Tsytovich, and G. Morfill, Physics of Plasmas **13**, 072104 (2006).
[23] S. A. A. and V. S. V., Contributions to Plasma Physics **49**, 260.
[24] K. Qiao, L. S. Matthews, and T. W. Hyde, IEEE Transactions on Plasma Science **38**, 826 (2010).
[25] V. Nosenko, A. V. Ivlev, R. Kompaneets, and G. Morfill, Physics of Plasmas **21**, 113701 (2014).
[26] J. Kong, T. W. Hyde, B. Harris, K. Qiao, and J. Carmona-Reyes, IEEE Transactions on Plasma Science **37**, 1620 (2009).
[27] J. Kong, K. Qiao, L. S. Matthews, and T. W. Hyde, Phys. Rev. E **90**, 013107 (2014).
[28] A. K. Mukhopadhyay and J. Goree, Phys. Rev. Lett. **109**, 165003 (2012).
[29] A. K. Mukhopadhyay and J. Goree, Phys. Rev. E **90**, 013102 (2014).
[30] A. V. Ivlev, R. Sütterlin, V. Steinberg, M. Zuzic, and G. Morfill, Phys. Rev. Lett. **85**, 4060 (2000).
[31] C. Zafiu, A. Melzer, and A. Piel, Phys. Rev. E **63**, 066403 (2001).
[32] Y.-N. Wang, L.-J. Hou, and X. Wang, Phys. Rev. Lett. **89**, 155001 (2002).
[33] D. P. Resendes, G. Sorasio, and P. K. Shukla, Physica Scripta **2002**, 87 (2002).
[34] D. P. Resendes, G. Sorasio, and P. K. Shukla, Physica Scripta **2002**, 87 (2002).
[35] K. Qiao, Z. Ding, J. Kong, M. Chen, L. S. Matthews, and T. W. Hyde, arXiv (2017).
[36] A. H. Nayfeh and D. T. Mook, (1979), 10.1002/9783527617586.
[37] P. S. Epstein, Phys. Rev. **23**, 710 (1924).
[38] M. Chen, M. Dropmann, B. Zhang, L. S. Matthews, and T. W. Hyde, Phys. Rev. E **94**, 033201 (2016).
[39] A. Douglass, V. Land, K. Qiao, L. Matthews, and T. Hyde, Journal of Plasma Physics **82**, 615820402 (2016).
[40] E. B. Tomme, D. A. Law, B. M. Annaratone, and J. E. Allen, Phys. Rev. Lett. **85**, 2518 (2000).
[41] E. B. Tomme, B. M. Annaratone, and J. E. Allen, Plasma Sources Science and Technology **9**, 87 (2000).
[42] N. J. Prior, L. W. Mitchell, and A. A. Samarian, Journal of Physics D: Applied Physics **36**, 1249 (2003).
[43] M. Lampe, G. Joyce, G. Ganguli, and V. Gavrishchaka, Physics of Plasmas **7**, 3851 (2000).
[44] F. Jenko, G. Joyce, and H. M. Thomas, Physics of Plasmas **12**, 022309 (2005).
[45] U. Konopka, G. E. Morfill, and L. Ratke, Phys. Rev. Lett. **84**, 891 (2000).
[46] P. Ludwig, W. J. Miloch, H. Kählert, and M. Bonitz, New Journal of Physics **14**, 053016 (2012).